# Divalent Ion Binding Properties of the Timothy Grass Allergen, Phl p 7[†]

Michael T. Henzl,* Meredith E. Davis, and Anmin Tan

*Department of Biochemistry, University of Missouri, Columbia, Missouri 65211*

*Received April 8, 2008; Revised Manuscript Received May 22, 2008*

ABSTRACT: The timothy grass allergen, Phl p 7, was studied by calorimetry, spectroscopy, and analytical ultracentrifugation. As judged by isothermal titration calorimetry (ITC), the protein binds $Ca^{2+}$ cooperatively with stepwise macroscopic association constants of $1.73 \times 10^6$ and $8.06 \times 10^6$ $M^{-1}$. By contrast, $Mg^{2+}$ binding is sequential with apparent macroscopic association constants of $2.78 \times 10^4$ and 170 $M^{-1}$. Circular dichroism and ANS fluorescence data suggest that $Ca^{2+}$ binding provokes a major conformational change that does not occur upon $Mg^{2+}$ binding. Conformational stability was assessed by differential scanning calorimetry (DSC). In phosphate-buffered saline (PBS) containing EDTA, the apoprotein undergoes two-state denaturation with a $T_m$ of 78.4 °C. In the presence of 0.02 mM $Ca^{2+}$, the $T_m$ exceeds 120 °C. Phl p 7 is known to crystallize as a domain-swapped dimer at low pH. However, analytical ultracentrifugation data indicate that the protein is monomeric in neutral solution at concentrations exceeding 1.0 mM, in both the apo and $Ca^{2+}$-bound states.

Type I hypersensitivity reactions are triggered by antigen-mediated cross-linking of receptor-bound IgE molecules on the surface of mast cells or basophils (*1*). The IgE cross-linking event leads to the release of histamine and leukotrienes and the subsequent onset of clinical symptoms (e.g., rhinoconjunctivitis, asthma, dermatitis, or anaphylactic shock). It is estimated that 25% of the population of the industrialized world is impacted by this disease process (*2, 3*). For many individuals, plant pollens are the primary allergen source.

Some of the most potent pollen allergens belong to the EF-hand protein family (*4–6*). The members of this large class of $Ca^{2+}$ binding proteins are critical components in eukaryotic signal transduction pathways, either serving explicitly as $Ca^{2+}$-dependent regulatory proteins (e.g., calmodulin) or indirectly influencing processes by buffering cytosolic $Ca^{2+}$ levels (e.g., parvalbumin). They are distinguished by their characteristic metal ion-binding motif, which consists of a central ion-binding loop flanked by short segments of helix (*5–7*). It was the recognition that the spatial orientation of these structural elements could be mimicked with the right hand that led Kretsinger to label this arrangement the "EF-hand" (*7–9*). Within the central loop, the coordinating ligands exhibit pseudo-octahedral symmetry and are indexed by a Cartesian axis system (*10*). A main chain carbonyl serves as the $-y$ ligand; the $-z$ ligand is a nearly invariant glutamate residue, and the $-x$ ligand is commonly a water molecule. The three remaining ligands are side chain oxygen atoms.

Plant allergens containing either two, three, or four EF-hands have been identified (*4, 5*). Expression of the two-EF-hand proteins, termed polcalcins, is evidently restricted to anthers and pollen (*11–14*). The observed enrichment at the tip of growing pollen tubes suggests a role for polcalcins in regulating the direction of pollen tube growth (*15*). Although IgE reactivity toward these proteins is observed in only a small subset (≤20%) of patients with pollen sensitivity (*16*), polcalcins exhibit marked allergenic potency in affected individuals (*17*). IgE antibodies to polcalcins reportedly exhibit greater affinity for the $Ca^{2+}$-bound state of the protein (*11, 16, 17*). Approximately 65% sequence identity is observed between polcalcins from different sources (*18*).

High-resolution structures have been published for several of the two-EF-hand proteins. In addition to the four helices associated with the two EF-hand motifs, the polcalcin secondary structure includes a highly conserved 11-residue helical segment at the C-terminus that is apparently unique to this class of proteins. Bet v 4, the structure of which was determined by NMR[1] spectroscopy, is monomeric, even at the high concentrations (0.7−1.5 mM) employed for the structure determination (*18*). By contrast, Phl p 7 and Che a 3 both crystallized as domain-swapped dimers (*19, 20*). The primary structures of Bet v 4, Phl p 7, and Che a 3 are compared in Figure 1A.

Our interest in Phl p 7 was originally sparked by the observation that the ligand constellation in EF-hand 2 is identical to that in the S55D and G98D variants of rat $\beta$-parvalbumin (Figure 1B). Although model peptide studies

[†] This work was supported by NSF Grant MCB0543476 (to M.T.H.).

* To whom correspondence should be addressed. Telephone: (573) 882-7485. Fax: (573) 884-4812. E-mail: henzlm@missouri.edu.

[1] Abbreviations: ANS, 1-anilinonaphthalene-8-sulfonic acid; CD, circular dichroism; CD site, parvalbumin metal ion binding site flanked by the C and D helical segments; DMPC, dimyristoylphosphatidylcholine; DPPC, dipalmitoylphosphatidylcholine; DSC, differential scanning calorimetry; DSPC, distearoylphosphatidylcholine; EDTA, ethylenediaminetetraacetic acid; EF site, parvalbumin metal ion binding site flanked by the E and F helical segments; EGTA, ethylene glycol bis($\beta$-aminoethyl ether)-*N*,*N*,*N*′,*N*′-tetraacetic acid; HBS, Hepes-buffered saline; Hepes, 4-(2-hydroxyethyl)-1-piperazineethanesulfonic acid; IPTG, isopropyl $\beta$-D-thiogalactopyranoside; ITC, isothermal titration calorimetry; LB, Luria-Bertani; NMR, nuclear magnetic resonance; NTA, nitrilotriacetic acid; PAGE, polyacrylamide gel electrophoresis; PBS, phosphate-buffered saline; THP, tris(hydroxypropyl)phosphine.

10.1021/bi800620g CCC: $40.75 
Published on Web 06/25/2008

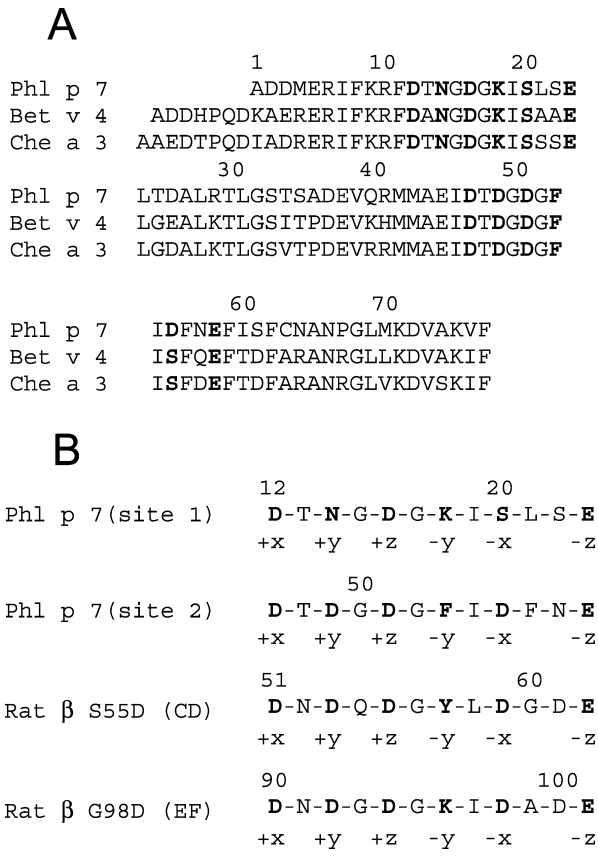


FIGURE 1: Primary structure of Phl p 7. (A) Comparison of amino acid sequences from Phl p 7, Bet v 4, and Che a 3. The residue numbers are those of Phl p 7. (B) Sequences of the $Ca^{2+}$ binding loops in Phl p 7. Note that the coordinating residues in site 2 are identical to those in the CD site of the S55D variant of rat $\beta$-parvalbumin and the EF site of the G98D variant.

had suggested that an EF-hand motif with five potential carboxylate ligands (aspartate at $+x$, $+y$, $+z$, and $-x$ and glutamate at $-z$) should exhibit reduced metal ion affinity (*21*), S55D and G98D displayed elevated affinity for $Ca^{2+}$ and $Mg^{2+}$ (*22*). This ligand array behaved similarly when introduced into the rat α-parvalbumin binding sites (*23, 24*). Thus, examining the binding properties of this ligand constellation in an altogether different EF-hand family member was of interest.

This paper examines the divalent ion binding behavior of Phl p 7 by isothermal titration calorimetry and CD and fluorescence spectroscopy. We also examine the conformational stability of the protein by differential scanning calorimetry and investigate its quaternary structure by analytical ultracentrifugation.

## MATERIALS AND METHODS

*Reagents and Chemicals.* NaCl, Hepes, $CaCl_2 \cdot H_2O$, $MgCl_2 \cdot 2H_2O$, $NaH_2PO_4$, EGTA, NTA, $Na_2EDTA \cdot 2H_2O$, lysozyme, Spectrapor 1 dialysis tubing (MWCO of 6000−8000), *N*,*N*′-methylene-bisacrylamide, and acrylamide were purchased from Fisher Scientific Co. LB agar, LB broth, and ampicillin were obtained from Research Products International. IPTG and DTT were purchased from Gold Biotechnology. DEAE-Sepharose, Sephadex G-75, THP, and ANS were obtained from Sigma-Aldrich Co.

*Expression and Purification of Phl p 7.* The Phl p 7 coding sequence, optimized for expression in *Escherichia coli*, was synthesized by GenScript Corp. (Piscataway, NJ) and subcloned into pET11a (Novagen), between the NdeI and BamHI sites. *E. coli* BL21(DE3) cells harboring that construct were cultured in LB broth containing ampicillin (100 $\mu$g/mL). Protein expression was induced with IPTG (0.25 mM) when the absorbance at 600 nm reached 0.6, and incubation was continued for an additional 16 h. The bacteria were harvested by centrifugation and resuspended in 5 volumes of 20 mM Hepes (pH 7.4). Lysis was achieved by lysozyme treatment (15 min, 37 °C, 5 mg of lysozyme/g of cell paste), followed by extrusion from a French pressure cell. Cell debris was removed by centrifugation for 30 min at 27000*g*. This step and subsequent purification steps were performed at 4 °C.

The clarified lysate was diluted with an equal volume of cold deionized water and loaded onto DEAE-Sepharose (4 mL/g of cell paste), pre-equilibrated with 20 mM Hepes (pH 7.4). The column was eluted, at a flow rate of 0.5 mL/min, with a linear NaCl gradient (from 0 to 0.6 M, 10 column bed volumes). Fractions containing Phl p 7, identified by nondenaturing PAGE, were combined, concentrated to a volume of 6 mL, and loaded onto Sephadex G-75, pre-equilibrated with 0.15 M NaCl and 0.025 M Hepes (pH 7.4) (Hepes-buffered saline). Fractions containing Phl p 7 were identified by absorbance spectroscopy.

With Phl p 7 lacking tyrosine and tryptophan, its UV spectrum exhibits the characteristic vibronic structure of phenylalanine and serves as a stringent indicator of homogeneity. Because the material collected from the gel filtration column displayed significant absorbance at 280 nm, it was subjected to a second round of anion-exchange chromatography, in the presence of EDTA. Following dialysis against 20 mM Hepes and 1 mM EDTA (pH 7.4), the protein was loaded onto DEAE-Sepharose that had been equilibrated with the same buffer and then eluted with a 0 to 0.6 M NaCl gradient. The purity of the resulting material exceeded 98%. The molecular mass, determined by MALDI-TOF mass spectrometry, was 8545.5 ± 1.2 Da, in excellent agreement with the predicted molecular mass for Phl p 7 lacking the initiating methionine residue. Protein concentrations were estimated spectrophotometrically, employing a molar extinction coefficient at 257 nm of 1400 $M^{-1}$ $cm^{-1}$.

*Spectroscopy.* Circular dichroism (CD) data were collected at 25 °C with an Aviv 62DS spectrometer. To compare the spectra of apo, $Ca^{2+}$-bound, and $Mg^{2+}$-bound Phl p 7, the $Ca^{2+}$-free protein was diluted to 50 $\mu$M in Hepes-buffered saline containing 1.0 mM EDTA, 200 $\mu$M $Ca^{2+}$, or 1.0 mM $Mg^{2+}$ and 1.0 mM EGTA. Inclusion of EGTA in the $Mg^{2+}$-containing solution ensures that contaminating $Ca^{2+}$ will not be bound by the protein. Data were collected at 1 nm intervals between 250 and 200 nm in a 0.10 cm quartz cuvette, averaging each data point for 5 s.

The emission spectrum of ANS was studied in the absence and presence of Phl p 7 with an SLM-Aminco 8100 fluorometer, modified (by ISS Inc., Champagne, IL) for photon counting. Data were collected at 1 nm intervals between 380 and 600 nm, using VINCI data acquisition software (ISS), averaging for 1 s at each point. The excitation wavelength was 365 nm. A bandpass of 4 nm was employed for both excitation and emission channels. Except for the fact that the emission signal is divided by the reference channel output, the spectra are uncorrected.

A nominal 1.0 mM solution of ANS was prepared in Hepes-buffered saline and standardized spectrophotometrically using an extinction coefficient of 4950 $M^{-1}$ $cm^{-1}$ (*25*). The stock solution was subsequently diluted to 10 $\mu$M in HBS containing either 200 $\mu$M $Ca^{2+}$, 50 mM EDTA, or 1.0 mM $Mg^{2+}$ and 10 mM EGTA. After the spectrum of ANS alone had been collected, additions of 1.0 mM $Ca^{2+}$-free Phl p 7 were made to yield final protein concentrations of 25, 50, 75, and 100 $\mu$M. Data were collected at 25 °C in a 1.0 cm quartz cuvette.

*Sedimentation Equilibrium.* Analyses were conducted at 20 °C in a Beckman XL-I analytical ultracentrifuge. Prior to analysis, protein samples were dialyzed extensively against the reference buffer, HBS containing either 5.0 mM EDTA or 100 $\mu$M $Ca^{2+}$. The final dialysis solution also contained 1.0 mM tris(hydroxypropyl)phosphine (THP). Sedimentation was conducted in six-sector charcoal-Epon centerpieces, which permit simultaneous examination of three loading concentrations in a single cell. Radial solute distributions, monitored at 257 nm, were collected at 1 h intervals until successive data sets were indistinguishable. Typically, 10 absorbance readings were averaged at each radial position. Data were collected at 20000, 30000, and 40000 rpm.

The absorbance profiles for all nine sample−solvent pairs were subjected to simultaneous (global) weighted nonlinear least-squares analysis in Origin version 7.5 (OriginLab). The data were satisfactorily accommodated by an equation describing the radial distribution of a single ideal species:

$$a = a_o \exp\left[\frac{M\omega^2(1-\bar{v}\rho)}{2RT}\left(r^2 - r_o^2\right)\right] + \mathrm{bl} \qquad (1)$$

where $a$ is the absorbance at radial position $r$, $a_o$ is the absorbance at an arbitrary reference position $r_o$, $M$ is the molecular weight, P is the angular velocity, $\bar{v}$ is the partial specific volume, $\rho$ is the solution density, $R$ is the gas constant, $T$ is the absolute temperature, and bl is a baseline offset to account for optical mismatch between the sample and solvent sectors. The partial specific volume was assumed to be 0.73 $cm^3$/g, and the solvent density was measured with an Anton-Paar DMA 5000 densitometer.

*Sedimentation Velocity.* Following dialysis against Hepes-buffed saline, containing 100 $\mu$M $Ca^{2+}$, Phl p 7 (5.8 mg/mL) and buffer were loaded into the sample and reference chambers, respectively, of a charcoal-Epon dual-sector centerpiece. After the rotor had equilibrated at 20 °C for 2 h under vacuum, the centrifuge was accelerated to 45000 rpm. Data acquisition was initiated immediately upon reaching speed and continued until 150 radial absorbance scans had been collected. The continuous $c(s)$ and $c(M)$ distributions were obtained with Sedfit (*26*) version 9.4.

*Isothermal Titration Calorimetry.* Prior to analysis, residual $Ca^{2+}$ was removed from the Phl p 7 preparation by treatment with EDTA-derivatized agarose (*27, 28*). An 80 $\mu$M solution (30 mL) of the protein was passed through a 90 mL column of EDTA-agarose, equilibrated with 0.15 M NaCl and 0.025 M Hepes (pH 7.4), at a flow rate of 0.5 mL/min, at 4 °C. The resulting material contained <0.02 molar equiv of $Ca^{2+}$, as determined by flame atomic absorption spectrometry. Similarly treated buffer contained undetectable levels of $Ca^{2+}$ (<0.2 $\mu$M).

ITC experiments were conducted in 0.15 M NaCl and 0.025 M Hepes (pH 7.4) at 25 °C, employing a VP-ITC calorimeter (MicroCal, LLC). Following thermal equilibration, titrant was added to the 1.41 mL sample at 240 s intervals. All titration protocols included a 2 $\mu$L preaddition, the heat from which was neglected during data analysis. $Ca^{2+}$ and $Mg^{2+}$ concentrations were determined by titrating standard EDTA solutions, prepared from analytical reagent-grade $Na_2EDTA \cdot 2H_2O$.

Samples of protein (typically 50−60 $\mu$M) were titrated with $Ca^{2+}$ in the presence and absence of competitive chelators (EDTA, EGTA, and NTA) or $Mg^{2+}$ and with $Mg^{2+}$ in the presence and absence of EDTA.

Following integration of the raw data, using software supplied with the instrument, the resulting composite data set was subjected to simultaneous least-squares minimization, to yield estimates of the binding constants and enthalpies for both $Ca^{2+}$ and $Mg^{2+}$. Aspects of the data treatment, including evaluation of parameter uncertainties, have been described in detail previously (*29, 30*).

The binding of $Ca^{2+}$ to Phl p 7 evidently occurs with positive cooperativity, necessitating the use of macroscopic binding constants. After the $i$th titrant addition, the cumulative heat (in microcalories) for $Ca^{2+}$ binding, in the absence of $Mg^{2+}$ or a competing chelator, is described by the equation

$$Q_i = 10^6 V P_t \left[\frac{\Delta H_1 K_1 [Ca^{2+}] + (\Delta H_1 + \Delta H_2) K_2 K_1 [Ca^{2+}]^2}{1 + K_1[Ca^{2+}] + K_2 K_1 [Ca^{2+}]^2}\right] \qquad (2)$$

where $V$ is the sample cell volume, $P_t$ is the total protein concentration, $\Delta H_1$ and $\Delta H_2$ are the binding enthalpies for the first and second binding events, respectively, and $K_1$ and $K_2$ are the first and second stepwise binding constants, respectively. The same equation can also be used to treat the binding of $Mg^{2+}$ in the absence of competing chelator.

If $Mg^{2+}$ is present, the numerator in eq 2 is modified to include the contribution from a mixed $Ca^{2+}-Mg^{2+}$ complex, the formation of which is governed by an overall binding constant $\beta_{CM}$. In addition, the denominator, i.e., the binding partition function, is expanded to include the mixed complex and the singly and doubly bound $Mg^{2+}$ complexes.

$$Q_i = 10^6 V P_t \left[\frac{\begin{array}{c}\Delta H_1 K_1 [Ca^{2+}] + (\Delta H_1 + \Delta H_{2M}) \beta_{CM} [Ca^{2+}][Mg^{2+}] + \\ \Delta H_1 K_1 [Ca^{2+}] + (\Delta H_1 + \Delta H_{2M}) \beta_{CM} [Ca^{2+}][Mg^{2+}] + \\ (\Delta H_1 + \Delta H_2) K_2 K_1 [Ca^{2+}]^2\end{array}}{\begin{array}{c}1 + K_1[Ca^{2+}] + K_{1M}[Mg^{2+}] + \beta_{CM}[Ca^{2+}][Mg^{2+}] + \\ K_2 K_1 [Ca^{2+}]^2 + K_{2M} K_{1M} [Mg^{2+}]^2\end{array}}\right] \qquad (3)$$

This model assumes that the enthalpy associated with formation of the mixed complex is adequately approximated by the sum of the enthalpies for the first $Ca^{2+}$ binding event and the second $Mg^{2+}$ binding event.

In the presence of a competing chelator, such as EDTA, eq 2 is modified to yield

$$Q_i = 10^6 V \left\{ P_t \left[\frac{\Delta H_1 K_1 [Ca^{2+}] + (\Delta H_1 + \Delta H_2) K_2 K_1 [Ca^{2+}]^2}{1 + K_1[Ca^{2+}] + K_2 K_1 [Ca^{2+}]^2}\right] + I_t \frac{\Delta H_I K_I [Ca^{2+}]}{1 + K_I [Ca^{2+}]} \right\} \qquad (4)$$

where $I_t$ is the total chelator concentration and $\Delta H_I$ and $K_I$ are the binding enthalpy and formation constant for the $Ca^{2+}$−inhibitor complex, respectively.

The injection heat for the *i*th addition is modeled as the difference between the cumulative heats associated with the *i*th and $(i - 1)$th additions:

$$q_i = (Q_i - Q_{i-1}) + \left(\frac{dV_i}{V}\right)\left(\frac{Q_i + Q_{i-1}}{2}\right) \quad (5)$$

The second term in eq 5 is a correction for the heat associated with the volume of solution displaced from the sample cell by the *i*th titrant addition, where $dV_i$ is the volume of that injection.

*Differential Scanning Calorimetry (DSC).* DSC was performed in a modified Nano-DSC device (Calorimetry Sciences Corp.) equipped with cylindrical hastalloy cells, having nominal volumes of 0.32 mL. Temperature calibration was verified with DMPC, DPPC, and DSPC. The accuracy of the differential power measurements was verified with internally generated electrical calibration pulses.

Samples were dialyzed extensively against 0.15 M NaCl, 0.01 M $NaP_i$, and 0.005 M EDTA (pH 7.4) (PBS/EDTA), which then served as the reference solution. The sample and reference solutions were degassed briefly under vacuum prior to loading. A scan rate of 60 °C/h was employed for all experiments. Phl p 7 exhibits an exotherm on the cooling scan and an endotherm on rescan, indicating reversible denaturation. A baseline, obtained with sample and reference cells filled with buffer, was subtracted from the protein data prior to analysis. Data collected at several protein concentrations were subjected to global nonlinear least-squares analysis to extract estimates of $T_m$, $\Delta H_{cal}$, $\Delta H_{vH}$, and $\Delta C_p$, as described previously (*31*). The conformational stability at 25 °C was estimated using the integrated Gibbs−Helmholtz equation:

$$\Delta G(T) = \Delta H_{vH}(T_m)(1 - T/T_m) + \Delta C_p[(T - T_m) - T\ln(T/T_m)] \quad (6)$$

To examine the impact of $Ca^{2+}$ on the stability of Phl p 7, material was first dialyzed extensively against Hepes-buffered saline containing 0.005 M EDTA and then against three changes of HBS containing 20 $\mu$M $Ca^{2+}$.

## RESULTS

*Isothermal Titration Calorimetry.* Representative titrations of Phl p 7 with $Ca^{2+}$ and $Mg^{2+}$ are displayed in panels A and B of Figure 2, respectively. Notice that the appearance of the $Ca^{2+}$ titration suggests that the second binding event is more exothermic than the first. In addition to these experiments, the protein was also titrated with $Ca^{2+}$ in the presence of $Mg^{2+}$ (1.0, 5.0, and 10.0 mM), with $Ca^{2+}$ in the presence of competing chelators (EDTA, EGTA, or NTA), and with $Mg^{2+}$ in the presence of EDTA. The integrated data for these titrations, displayed in Figure 3, were compiled into a single data set and subjected to weighted least-squares minimization, to extract estimates of the binding constants and binding enthalpies for $Ca^{2+}$ and $Mg^{2+}$.

The best fit to the data is indicated by the solid lines in Figure 3. The optimal parameter values are listed in Table 1, and the energetics of divalent ion binding at 25 °C are summarized in Table 2. At $8.1 \times 10^6$ $M^{-1}$, $K_2$ is approximately 5 times larger than $K_1$, indicating that $Ca^{2+}$ binding occurs with positive cooperativity. By contrast, $Mg^{2+}$ binding is clearly sequential, and the two $Mg^{2+}$ binding constants, $2.77 \times 10^4$ and 170 $M^{-1}$, are markedly dissimilar. The least-squares fit is modestly improved by including a mixed $Ca^{2+}$−$Mg^{2+}$ species in the partition function, which presumably reflects occupancy of the high-affinity $Ca^{2+}$ site and the low-affinity $Mg^{2+}$ site. The formation constant for this complex, $\beta_{CM}$, is estimated to be $1.08 \times 10^9$ $M^{-2}$.

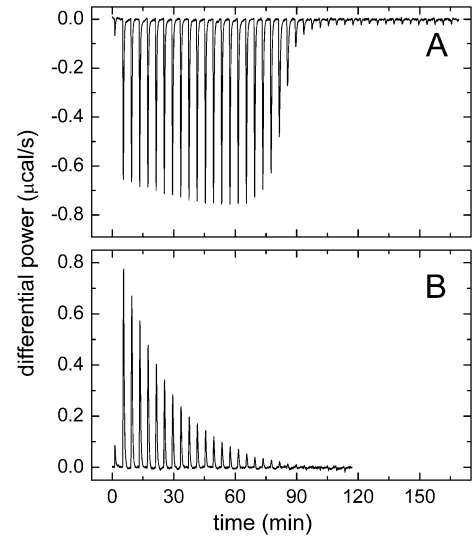


FIGURE 2: Raw ITC data. Representative data are shown for the titration of 60 $\mu$M Phl p 7 with 1.10 mM $Ca^{2+}$ (A) and 1.98 mM $Mg^{2+}$ (B). Both experiments were conducted at 25 °C, in Hepes-buffered saline (pH 7.4).

The binding constants extracted from the ITC data were used to calculate the fraction of protein present in the apo, singly ligated, and doubly ligated forms as a function of free $Ca^{2+}$ concentration (Figure 4). Note that formation of the doubly ligated species is strongly suppressed by 1 mM $Mg^{2+}$ (dotted line). However, if a hypothetical target protein (10 $\mu$M), having a binding constant of $10^7$ $M^{-1}$ for $Ca^{2+}$-bound Phl p 7, is also included in the calculation, the species fraction curve is shifted back into the physiologically relevant range (dashed line).

*ANS Fluorescence.* The positively cooperative $Ca^{2+}$ binding behavior suggested that the initial binding event in Phl p 7 is linked to a conformational change. To obtain corroborative evidence and to ascertain whether $Ca^{2+}$ binding is accompanied by exposure of apolar surface area, we examined the influence of Phl p 7 on ANS fluorescence. The quantum yield of ANS increases dramatically with a decrease in solvent polarity, and the dye has a long history as a sensitive probe of solvent-accessible apolar surface on proteins (*32*). In Hepes-buffered saline, at pH 7.4, the spectrum exhibits a broad maximum at 530 nm and a sharper feature at 498 nm. Addition of $Ca^{2+}$-bound Phl p 7 produces a marked increase in fluorescence at 498 nm (Figure 5A).

If the same experiment is conducted in the presence of 1.0 mM $Mg^{2+}$ and 10 mM EGTA, a much smaller increase in fluorescence is observed (Figure 5B) over the same Phl p 7 concentration range. In fact, the increase observed in the presence of $Mg^{2+}$ and EGTA is comparable to that observed in the presence of excess EDTA (Figure 5C). The intensity of the emission at 498 nm is displayed as a function of Phl p 7 concentration in Figure 5D for the three different solution

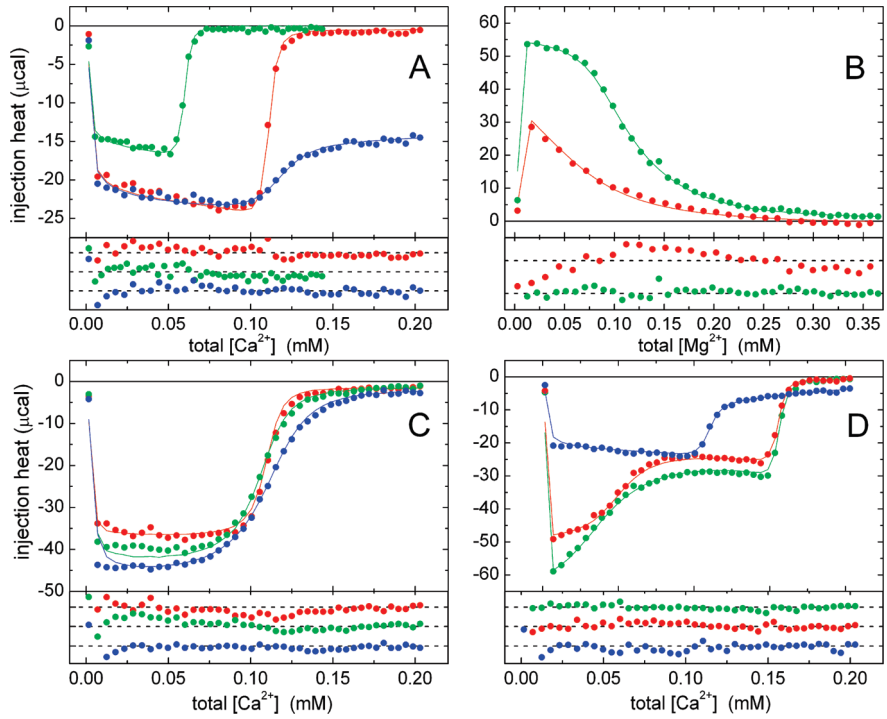


FIGURE 3: Analysis of divalent ion binding by global least-squares analysis of ITC data. Samples of Phl p 7 were subjected to a battery of titrations as described in Materials and Methods. The integrated data from those experiments are displayed in the top panels. The solid lines through the data reflect the best least-squares fit to the data ($\chi^2 = 5.14$), and the residuals for that fit are shown in the bottom panels: (A) 1.1 mM $Ca^{2+}$ vs 60 $\mu$M Phl p 7 (red), 30 $\mu$M Phl p 7 (green), and 60 $\mu$M Phl p 7 and 1.0 mM NTA (blue); (B) 1.98 mM $Mg^{2+}$ vs 60 $\mu$M Phl p 7 (red) and 60 $\mu$M Phl p 7 and 100 $\mu$M EDTA (green); (C) 1.1 mM $Ca^{2+}$ vs 59.5 $\mu$M Phl p 7 and 1.0 mM $Mg^{2+}$ (red), 57.7 $\mu$M Phl p 7 and 5.0 mM $Mg^{2+}$ (green), and 61.3 $\mu$M Phl p 7 and 10.0 mM $Mg^{2+}$ (blue); and (D) 1.1 mM $Ca^{2+}$ vs 60 $\mu$M Phl p 7 and 60 $\mu$M EDTA (red), 60 $\mu$M Phl p 7 and 60 $\mu$M EGTA (green), and 60 $\mu$M Phl p 7 and 100 $\mu$M NTA (blue).

Table 1: Characterization of Phl p 7

| | value | 95% confidence interval |
|---|---|---|
| $Ca^{2+}$ binding parameters | | |
| $\Delta H_1$ | −1.85 kcal/mol | −1.96 to −1.59 |
| $K_1$ | $1.73 \times 10^6$ $M^{-1}$ | 1.51−1.97 |
| $\Delta H_2$ | −4.00 kcal/mol | −4.11 to −3.68 |
| $K_2$ | $8.06 \times 10^6$ $M^{-1}$ | 6.77−9.35 |
| $Mg^{2+}$ binding parameters | | |
| $\Delta H_{1M}$ | 2.79 kcal/mol | 2.63−2.93 |
| $K_{1M}$ | $2.77 \times 10^4$ $M^{-1}$ | 2.36−3.11 |
| $\Delta H_{2M}$ | 5.68 kcal/mol | 5.22−6.08 |
| $K_{2M}$ | 170 $M^{-1}$ | 147−197 |
| $\beta_{Ca,Mg}$ | $1.08 \times 10^9$ $M^{-2}$ | 0.49−1.55 |
| thermal stability (apoprotein) | | |
| $T_m$ | 351.5 K | 351.1−351.7 |
| $\Delta H_{cal}$ | 54.5 kcal/mol | 52.2−54.8 |
| $\Delta H_{vH}$ | 55.6 kcal/mol | 55.5−56.5 |
| $\Delta C_p$ | 0.20 kcal $mol^{-1}$ $K^{-1}$ | 0.14−0.36 |
| $\Delta G_{conf}$ ($Ca^{2+}$-free, 25 °C) | 7.4 kcal/mol | 6.1−8.0 |
| $T_m$ (5 mM acetate, 0.5 mM EGTA) | 346.0 K | 345.8−346.2 |
| sedimentation | | |
| MW (apoprotein) | 8560 | 8460−8660 |
| MW ($Ca^{2+}$-bound) | 8570 | 8470−8670 |
| $s_w^{20}$ | 1.08 S | 1.06−1.10 |

conditions. Note that the lines defined by the data collected in $Mg^{2+}$ with EGTA and in EDTA are virtually coincident.

*Circular Dichroism.* The far-UV circular dichroism spectrum of Phl p 7 was examined as a function of its divalent ion binding status. The spectrum of apo-Phl p 7 is indicated by the hollow squares (□) in Figure 6. In the presence of 100 $\mu$M $Ca^{2+}$ (●), the features at 222 and 208 nm, correlated with helical structure, become perceptibly more pronounced. By contrast, the spectrum collected in the presence of 1.0 mM $Mg^{2+}$ and 1.0 mM EGTA (▲) can nearly be superimposed on that of the apoprotein.

*Sedimentation Equilibrium.* Samples of apo-Phl p 7, at nominal loading concentrations of 560, 280, and 140 $\mu$M, were sedimented to equilibrium at 20 °C, at rotor speeds of 20000, 30000, and 40000 rpm. The resulting radial distributions are depicted in Figure 7. These data were analyzed globally using a single-species model (eq 1). The optimal least-squares fit, indicated by the solid lines in Figure 5, returns a value of 8560 ± 100 for the molecular weight.

Corresponding data for the $Ca^{2+}$-bound protein are displayed in Figure 8. Treatment with the single-species model yielded an estimate of 8570 ± 100 for the molecular weight. The sequence-derived molecular weight of Phl p 7 is 8546.

*Sedimentation Velocity.* A sample of Phl p 7 having a nominal concentration of 0.76 mM was sedimented at 45000 rpm and 20 °C. The resulting 150-scan data set was analyzed with Sedfit (version 9.4). A subset of the 150 absorbance scans is displayed in Figure 9A, along with the optimal $c(s)$ fit; the corresponding residuals are displayed beneath the data. The distribution of sedimentation coefficients exhibits a single major peak, centered at approximately 1.08 S (Figure 9B). The corresponding peak in the $c(M)$ distribution (Figure 9C) is centered at 7800. A very broad, minor feature between 2.5 and 5.0 S in the $c(s)$ plot accounts for <0.7% of the entire area.

*Differential Scanning Calorimetry.* The intrinsic conformational stability of the protein was examined by DSC in PBS (pH 7.4) containing 0.005 M EDTA. Under these conditions, thermal denaturation is reversible. Data obtained at three different protein concentrations, 2.2, 4.3, and 6.5

Table 2: Thermodynamics of Divalent Ion Binding by Phl p 7 at 25 °C[a]

| | $Ca^{2+}$ binding | | | $Mg^{2+}$ binding | | |
|---|---|---|---|---|---|---|
| | $\Delta H$ | $-T\Delta S$[b] | $\Delta G$[c] | $\Delta H$ | $-T\Delta S$ | $\Delta G$ |
| binding event 1 | −1.85 | −6.65 | −8.50 | 2.79 | −8.85 | −6.06 |
| binding event 2 | −4.00 | −5.42 | −9.42 | 5.68 | −8.72 | −3.04 |
| total | −5.85 | −12.07 | −17.92 | 8.47 | −17.57 | −9.10 |

[a] All energies expressed in kilocalories per mole. [b] Calculated with the formula $-T\Delta S = \Delta G - \Delta H$. [c] Calculated with the formula $\Delta G = -RT \ln K$.

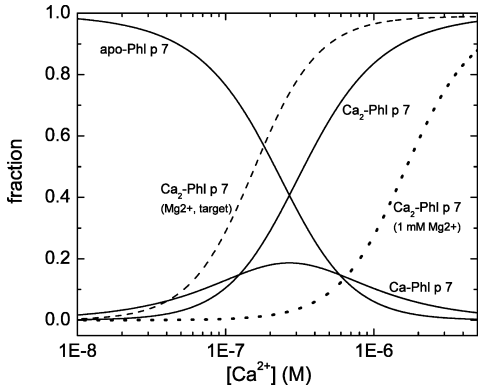


FIGURE 4: Population of the apo, singly bound, and doubly bound species of Phl as a function of free $Ca^{2+}$ concentration. The dotted line indicates the curve for the doubly bound species that would be observed in the presence of 1.0 mM $Mg^{2+}$, and the dashed line reflects the curve that would be obtained in the presence of 1.0 mM $Mg^{2+}$ and 10 $\mu$M putative target peptide having an apparent affinity constant of $10^8$ $M^{-1}$ for the doubly bound species.

mg/mL, are displayed in Figure 10. The denaturation was treated with a two-state model, to extract estimates of the melting temperature, the van't Hoff and calorimetric enthalpies, and the denaturational heat capacity increment. The analysis yielded these parameter values: 78.4 °C, 55.6 kcal/mol, 54.5 kcal/mol, and 0.20 kcal $mol^{-1}$ $K^{-1}$, respectively. At a low ionic strength [0.5 mM EGTA and 5.0 mM acetate (pH 6.0)], the $T_m$ is decreased by 5.0 °C (Figure 10, magenta circles).

As anticipated, the addition of $Ca^{2+}$ greatly stabilizes the protein. At a free $Ca^{2+}$ concentration of 20 $\mu$M, the transition midpoint is shifted to approximately 120 °C, as indicated by the cyan symbols in Figure 10.

## DISCUSSION

In the following paragraphs, we examine the topic of Phl p 7 quaternary structure, briefly discuss the issue of Phl p 7 conformational stability, and close with a discussion of the interesting divalent ion binding behavior.

*Quaternary Structure of Phl p 7.* EF-hand motifs typically occur in pairs, forming a globular EF-hand domain (*8*). Within this domain, which exhibits pseudo-2-fold symmetry, the two motifs are joined by a short segment of antiparallel $\beta$ structure. Thus, the dimeric crystal structure reported for Phl p 7 [Protein Data Bank (PDB) entry 1K9U] (*19*) is distinctly unusual. Within the dimer, each monomer assumes an extended conformation. Although the EF-hand motifs are paired, the pairing occurs between the N-terminal motif of one chain and the C-terminal motif of the other. This domain-swapped dimeric structure encloses a solvent-inaccessible hydrophobic cavity having a volume of 800 Å$^3$. Interestingly, the crystal structure of Che a 3 (PDB entry 2OPO) also exhibits this domain-swapped structure (*20*).

Significantly, however, our sedimentation analyses indicate that Phl p 7 is monomeric in Hepes-buffered saline, at pH 7.4. The equilibrium data, collected at three protein concentrations and three rotor speeds, can be satisfactorily modeled with the assumption of a single ideal species with a molecular weight of 8560 (apo) or 8570 ($Ca^{2+}$-bound). Furthermore, when a 0.76 mM sample is subjected to velocity analysis, the resulting distribution of sedimentation coefficients exhibits a symmetric peak at 1.08 S, which accounts for >99% of the area. The homologue of Phl p 7 from birch tree, Bet v 4, is likewise predominantly monomeric, with evidence of limited dimer formation observed only at very high protein concentrations (*18*). The peak in the $c(s)$ distribution for Bet v 4 occurs at 1.25 S, consistent with its somewhat higher molecular weight (9400).

The biological significance of domain-swapped structures has been questioned in other systems (*33*). Because $Ca^{2+}$-bound Phl p 7 was crystallized at pH 3.2−3.4, well below its isoelectric point (estimated to be 4.5), the domain-swapped dimer may represent a crystallization artifact. Of course, it is also conceivable that the dimer represents a physiologically relevant form of the protein that is only accessed, at neutral pH, in the presence of an appropriate target ligand. Further exploration of this issue is warranted.

The behavior of Phl p 7 in size-exclusion chromatography studies at pH 4.7 and 7.1 was cited as evidence of the physiological relevance of the domain-swapped structure (*19*). However, elution behavior in size-exclusion chromatography is strongly influenced by shape, as well as size. An ellipsoidal molecule will appear to be larger (i.e., elute earlier) than a spherical molecule with an identical molecular weight. In fact, one could argue that the (highly ellipsoidal) Phl p 7 dimer should exhibit an apparent molecular weight significantly larger than 14000. Our sedimentation analysis suggests that the size-exclusion studies were actually monitoring the behavior of the Phl p 7 monomer, with the inflated apparent molecular weight reflecting the departure of the molecule from spherical symmetry.

*Thermal Stability of Phl p 7.* $Ca^{2+}$-free Phl p 7 displays substantial thermal stability, with a $T_m$ in phosphate-buffered saline at pH 7.4 of 78.4 °C. Consistent with the sedimentation results, the DSC studies on Phl p 7 likewise provide no evidence of a dimeric species. The denaturation behavior can be satisfactorily accommodated with a two-state model. Two-state denaturation of a dimeric protein ($N_2 \rightarrow 2U$) would exhibit a $\Delta H_{vH}/\Delta H_{cal}$ ratio approaching 2.0. For Phl p 7, however, the ratio is 1.02, suggesting that the monomer is the unfolding unit and that denaturation occurs with a negligible population of partially unfolded intermediate states. The fact that thermal denaturation data collected at protein concentrations ranging from 2.2 to 6.5 mg/mL can be modeled with a common set of parameters ($T_m$, $\Delta H_{vH}$,

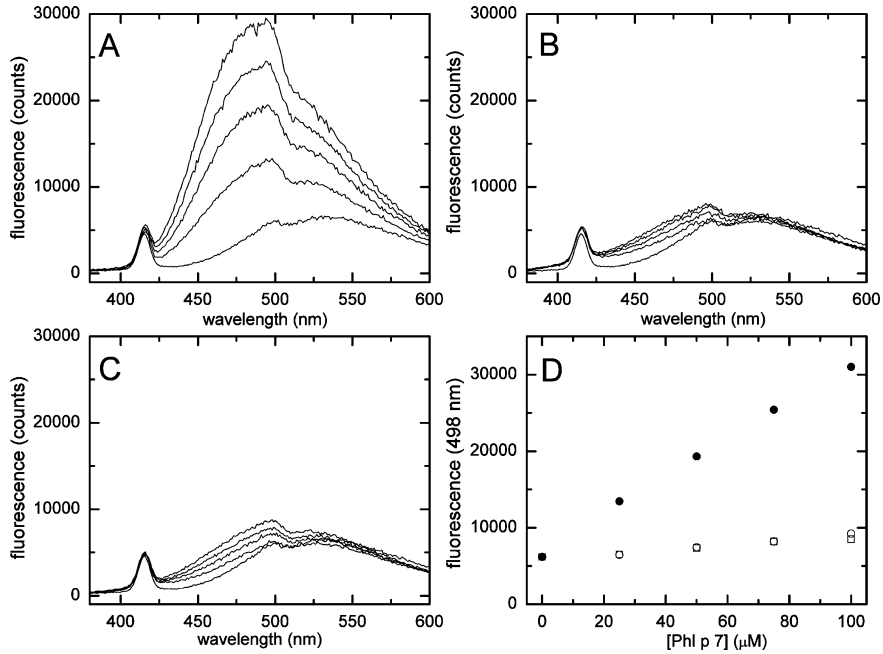


FIGURE 5: ANS fluorescence analysis. (A) ANS (10 $\mu$M) was examined in Hepes-buffered saline containing 200 $\mu$M $Ca^{2+}$, in the absence of Phl p 7 (bottom trace) and in the presence of 25, 50, 75, and 100 $\mu$M Phl p 7. (B) Data collection as described for panel A, except for the presence of 10 mM EGTA and 1.0 mM $Mg^{2+}$. (C) Data collection as described for panel A, except for the presence of 50 mM EDTA. The spectra in panels A−C are not corrected for dilution. The feature at 417 nm is due to Raman scattering from the solvent. Additional experimental details are provided in Materials and Methods. (D) Intensity of the ANS emission signal at 498 nm as a function of added Phl p 7, in the presence of 200 $\mu$M $Ca^{2+}$ (●), 1.0 mM $Mg^{2+}$ and 10 mM EGTA (○), and 50 mM EDTA (□).

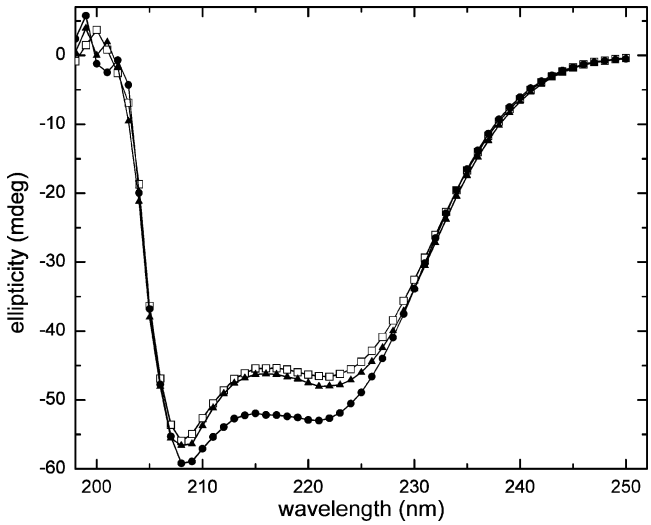


FIGURE 6: Far-UV circular dichroism spectra of Phl p 7. Data were collected, as described in Materials and Methods, for $Ca^{2+}$-bound (●), $Ca^{2+}$-free (□), or $Mg^{2+}$-bound (▲) Phl p 7.

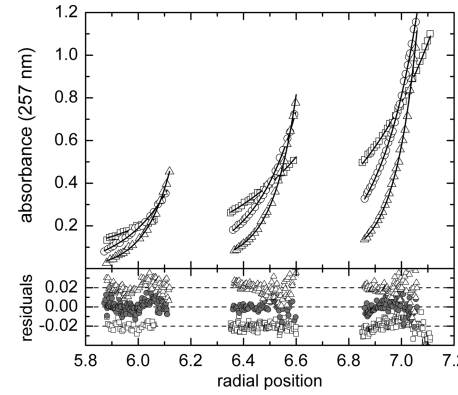


FIGURE 7: Sedimentation equilibrium analysis of $Ca^{2+}$-free Phl p 7. Following dialysis against Hepes-buffered saline containing 5.0 mM EDTA and 1 mM THP, samples of Phl p 7 were centrifuged to equilibrium, employing rotor speeds of 20000 (□), 30000 (○), and 40000 rpm (△). The nominal loading concentrations were 140, 280, and 560 $\mu$M. The solid lines represent the best least-squares fit to an ideal single-species model. For clarity, only a subset of the data points is displayed in the top panel. Residuals for the optimal fit are displayed in the bottom panel.

$\Delta H_{cal}$, and $\Delta C_p$) is further evidence that the quaternary structure of Phl p 7 is unchanged over this range.

The relatively high thermal stability of apo-Phl p 7 is a reflection of the diminutive $\Delta C_p$ for denaturation, 0.20 kcal $mol^{-1}$ $K^{-1}$. The value of $\Delta C_p$ is largely determined by the increase in solvent-accessible apolar surface area that accompanies unfolding. In this case, the magnitude of the denaturational heat capacity increment reflects the relatively small volume of the hydrophobic core. The extrapolated conformational stability for Phl p 7 at 25 °C is 7.4 kcal/mol.

Addition of $Ca^{2+}$ to Phl p 7 greatly increases its thermal stability. At a free $Ca^{2+}$ concentration of 20 $\mu$M, the $T_m$ exceeds 120 °C (cyan symbols, Figure 10), the high-temperature limit for our calorimeter. Bet v 4 likewise remains folded at temperatures approaching 100 °C (*18*).

Interestingly, the apo form of Bet v 4, a Phl p 7 homologue, reportedly unfolds at a much lower temperature, 45 °C in 5 mM sodium acetate and 0.5 mM EGTA (pH 6.0) (*18*). This difference is not, as we initially thought, a consequence of disparate experimental conditions. If Phl p 7 is analyzed under the same conditions, the melting temperature decreases to 72.9 °C, a decrease of just 5.5 °C. At present, an explanation for the disparate behavior of Phl p 7 and Bet v 4 cannot be given. With 69% sequence identity, it seems unlikely that the two proteins would possess significantly different intrinsic conformational stabilities.

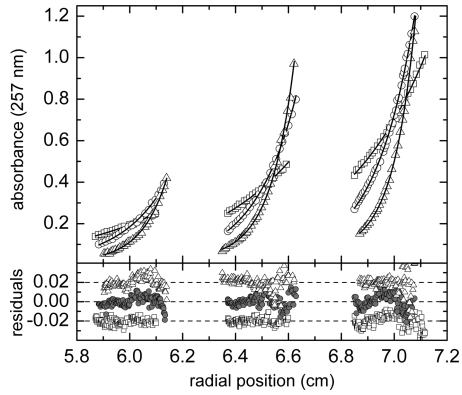


FIGURE 8: Sedimentation equilibrium analysis of $Ca^{2+}$-bound Phl p 7. Following dialysis against Hepes-buffered saline containing 100 $\mu$M $Ca^{2+}$ and 1 mM THP, samples of Phl p 7 were centrifuged to equilibrium, at rotor speeds of 20000 (□), 30000 (○), and 40000 rpm (△). The nominal loading concentrations were 140, 280, and 560 $\mu$M. The solid lines represent the best least-squares fit to an ideal single-species model. Residuals for the optimal fit are displayed in the bottom panel.

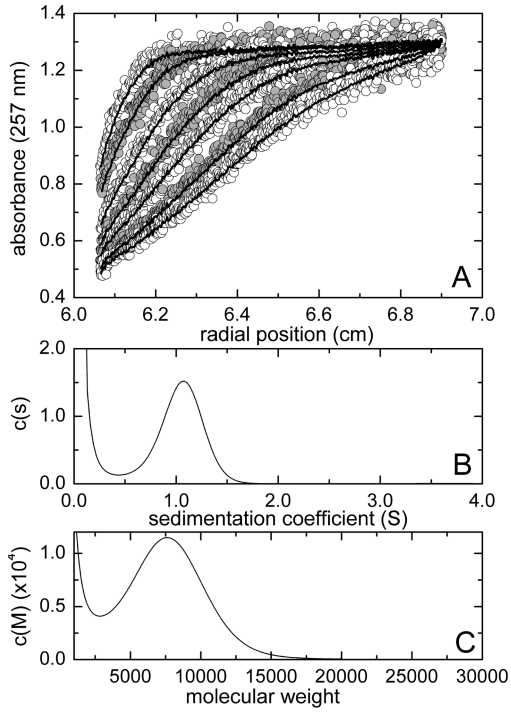


FIGURE 9: Sedimentation velocity analysis of $Ca^{2+}$-bound Phl p 7. A 760 $\mu$M sample of Phl p 7, in Hepes-buffered saline containing 100 $\mu$M $Ca^{2+}$, was centrifuged at 45000 rpm and 20 °C. Data collection was initiated immediately upon attaining speed. The resulting 150-scan data set was analyzed with Sedfit (*26*). (A) Subset of the raw data. The solid lines reflect the optimal least-squares fits. (B) Distribution of sedimentation coefficients obtained with Sedfit, employing the continuous $c(s)$ model. (C) Molecular weight distribution obtained with Sedfit, employing the continuous $c(M)$ model.

Structural data for the apoproteins could provide welcome insight into the issue.

*Divalent Ion Binding Properties of Phl p 7.* The observed stepwise macroscopic binding constants, $K_1$ and $K_2$, are $1.7 \times 10^6$ and $8.1 \times 10^6$ $M^{-1}$, respectively. In the absence of cooperativity, if the two sites were intrinsically equivalent, $K_2$ would equal $0.25K_1$. In this case, $K_2$ equals $4.8K_1$. Thus, the minimal coupling free energy equals $-RT$ ln(4.8/0.25), or −1.7 kcal/mol at 25 °C. Because the two sites are almost assuredly not equivalent (vide infra), the magnitude of the coupling energy may be substantially larger.

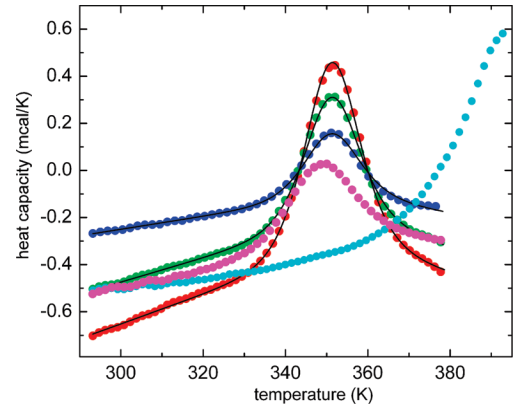


FIGURE 10: DSC analysis of Phl p 7. Samples of $Ca^{2+}$-free Phl p 7 were examined by DSC in PBS (pH 7.4) containing 5.0 mM EDTA. The protein concentrations were 2.2 (blue), 4.3 (green), and 6.5 mg/mL (red). For clarity, only a subset of the data points is presented. The data were analyzed with a two-state unfolding model, and the solid lines represent the best least-squares fit. Optimal parameter values are listed in Table 1. Data are also shown for the apoprotein, at 2.9 mg/mL, in 0.5 mM EGTA and 5.0 mM acetate (pH 6.0) (magenta) and for the $Ca^{2+}$-bound protein, at 4.3 mg/mL, in 0.15 M NaCl and 0.025 M Hepes containing 20 $\mu$M free $Ca^{2+}$ (cyan).

The appearance of positive cooperativity suggests that $Ca^{2+}$ binding is linked to a conformational transition, a hypothesis supported by spectroscopic data. With minima at 222 and 208 nm, the far-UV CD spectrum of apo-Phl p 7 is characteristic of a largely helical protein. Addition of $Ca^{2+}$ to a solution of Phl p 7 produces a significant increase in ellipticity, consistent with reorientation of helices and/or a minor increase in helical content (Figure 6). Similar behavior has been reported for other polcalcins (*11, 12, 15, 17, 34*).

ANS fluorescence measurements provide evidence of an alteration in tertiary structure. When Phl p 7 is added to a solution of ANS in the presence of 100 $\mu$M $Ca^{2+}$, the fluorescence of the dye increases markedly (Figure 5A). By contrast, when Phl p 7 is added in the presence of excess EDTA, ANS emission is essentially unchanged (Figure 5C). Evidently, $Ca^{2+}$ binding to Phl p 7 promotes a conformational change that results in exposure of apolar surface area. This finding is consistent with the high-resolution structure of $Ca^{2+}$-bound Bet v 4, which reveals a large hydrophobic groove (*18*). Although target peptides for the polcalcins have yet to be identified, the exposure of a large apolar surface upon $Ca^{2+}$ binding is clearly consistent with the regulatory role proposed for these proteins (*11, 18*).

The $Ca^{2+}$ binding behavior can be understood in terms of a classical allosteric model (*35*). The protein is assumed to reside in two distinct conformations, $M_0$ and $M_1$ (Scheme 1). Although, in principle, $Ca^{2+}$ can bind to either form, $M_1$ has a substantially higher affinity for the ion. The $M_0$ arm of the binding network is depicted in gray to reflect the lower affinity of $M_0$ for $Ca^{2+}$. The $M_0$−$M_1$ interconversion is governed by an equilibrium constant $L_1$, equal to $[M_1]/[M_0]$. Positive cooperativity arises when the apoprotein preferentially adopts the $M_0$ conformation ($L_1 < 1$). Binding of the first $Ca^{2+}$ ion is disfavored for two reasons. Because $K_{11} \gg K_{01}$, the ion binds primarily to the less abundant state of the protein. Moreover, because the majority of molecules must

Scheme 1

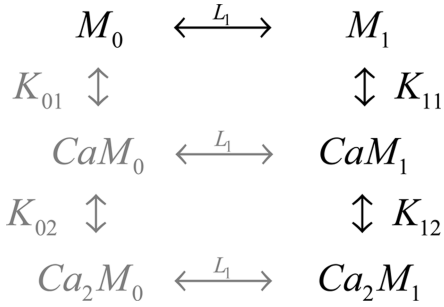


undergo conversion to $M_1$ prior to $Ca^{2+}$ binding, the net binding free energy is reduced by the energetic cost of the $M_0-M_1$ transition. By contrast, when the second $Ca^{2+}$ binds, the macromolecule resides almost exclusively in the $M_1$ state. Because there is no conformational energy penalty, the net free energy change for the second binding event can be more favorable than the first, even if the intrinsic affinity of the second site is lower than that of the first.

We propose that the first $Ca^{2+}$ is bound in site 2. The sequences of the two metal ion binding sites in Phl p 7 are displayed in Figure 1B, with the coordinating residues in boldface type. Site 2 includes five anionic residues: a glutamate at $-z$ and aspartates at $+x$, $+y$, $+z$, and $-x$. By contrast, site 1 harbors just three. In model peptide studies, EF-hand binding loops containing four anionic ligands bind $Ca^{2+}$ significantly more tightly than those having just three (*36–39*). A fifth anionic ligand has been shown to decrease metal ion affinity in model peptide systems (*21*), presumably due to an elevated level of electrostatic repulsion. However, engineered parvalbumin sites containing five anionic ligands, i.e., "pentacarboxylate" sites, exhibit heightened divalent ion affinity (*22, 23*).

Replacement of Ser-55 with aspartate in the CD site (residues 51−62) of rat $\beta$-parvalbumin increases $Ca^{2+}$ and $Mg^{2+}$ affinity by 1.7 and 3.2 kcal/mol, respectively. The corresponding variant of rat α-parvalbumin (S55D/E59D) exhibits 2.0 and 2.3 kcal/mol improvements, respectively. Introduction of a fifth anionic ligand into the EF site (residues 90−101), via the G98D mutation, has a more muted impact. $Ca^{2+}$ affinity increases significantly (1.3 and 1.1 kcal/mol in the rat α and $\beta$ isoforms, respectively), but $Mg^{2+}$ affinity is almost unchanged. Evidently, the influence of the additional anionic side chain can be modulated by the overall structural context.

The S55D variant of rat $\beta$-parvalbumin has resisted crystallization. However, the structure of the rat α S55D/E59D variant was recently determined (*24*). Although the CD site binding loop harbors five potential carboxylate ligands, only four participate in $Ca^{2+}$ coordination: $+x$, $+y$, $+z$, and $-z$ (bidentate). In wild-type rat $\beta$-parvalbumin, Asp-59 functions as an outer sphere ligand, coordinating $Ca^{2+}$ indirectly via the water molecule that serves as the proximal $-x$ ligand (*40*). However, judging from the structure of the α S55D/E59D variant, when Ser-55 is replaced with Asp at the $+z$ position, the Asp-59 carboxylate withdraws from the coordination sphere. Instead, it functions as a helix-capping residue for the D helix, forming a hydrogen bond with the backbone amide of Glu-62. The side chain of Asp-56 in Phl p 7 adopts a similar configuration, hydrogen bonding to the amide of Glu-59 (*19*). In view of the high-affinity signature displayed by this ligand array in the parvalbumin background, it is likely that site 2 is preferentially occupied by $Ca^{2+}$ in Phl p 7.

Given the striking resemblance of site 2 in Phl p 7 to the engineered pentacarboxylate sites in parvalbumin, it may seem surprising that the $Ca^{2+}$ association constant does not exceed $10^8$ M. The explanation lies in the disparate polcalcin and parvalbumin tertiary structures. As discussed earlier, $Ca^{2+}$ binding promotes exposure of a large apolar surface in Phl p 7, which carries a substantial energetic penalty. By contrast, the parvalbumin AB domain, formed by residues 1−38, completely occludes the hydrophobic aspect of the paired EF-hands. Because $Ca^{2+}$ binding is not accompanied by solvent exposure of a hydrophobic surface, the net $Ca^{2+}$ affinity of the pentacarboxylate ligand array can be substantially higher.

The unusual ligand array in site 2 (which first attracted our interest to Phl p 7) is not shared by all of the polcalcins. In the majority of the proteins, including Bet v 4, serine occupies the $-x$ position, rather than aspartate. It would be interesting to compare and contrast the divalent ion binding properties of a more typical polcalcin with those of Phl p 7.

$Ca^{2+}$ and $Mg^{2+}$ differ perceptibly in terms of their coordination by EF-hand motifs (*41*). The $-z$ glutamyl moiety binds $Ca^{2+}$ in a bidentate fashion so that the coordination geometry is actually pentagonal bipyramidal. Reflecting this difference, perhaps, $Mg^{2+}$ binding to Phl p 7 is sequential rather than cooperative, and the two sites exhibit highly disparate binding affinities, $2.78 \times 10^4$ and 170 $M^{-1}$. These binding results suggest that $Mg^{2+}$ does not promote the conformational change that accompanies $Ca^{2+}$ binding, and that hypothesis is supported by our CD and ANS fluorescence data. Unlike that of $Ca^{2+}$, the addition of $Mg^{2+}$ to Phl p 7 does not produce a significant increase in ellipticity at 222 and 208 nm. Moreover, ANS fluorescence is unchanged upon addition of Phl p 7 in the presence of $Mg^{2+}$. At the $Mg^{2+}$ concentration of 1.0 mM employed in these spectroscopic studies, the predicted occupancies of the high- and low-affinity sites in Phl p 7 should be approximately 97 and 15%, respectively.

Although $Mg^{2+}$ binding is macroscopically noncooperative, the global least-squares analysis suggests that binding of $Mg^{2+}$ at the weaker site is somewhat improved when $Ca^{2+}$ occupies the high-affinity site. In the absence of an interaction, the overall binding constant for the mixed $Ca^{2+}-Mg^{2+}$ complex would equal the product of the two stepwise constants, $K_1K_{2Mg}$, or $2.9 \times 10^8$ $M^{-1}$. In fact, the best-fit value for this parameter, $\beta_{CM}$, is 3.8 times larger, or $1.1 \times 10^9$ $M^{-2}$, corresponding to a coupling free energy of −0.79 kcal/mol. It is worth mentioning that this mixed complex would not be detectably populated at the concentrations of $Ca^{2+}$ and $Mg^{2+}$ present in vivo.

EF-hand motifs are commonly classified as either "$Ca^{2+}$/$Mg^{2+}$ sites" or "$Ca^{2+}$-specific sites". Well suited for $Ca^{2+}$ buffering roles, the former display high affinity for $Ca^{2+}$ ($K_{Ca} > 10^7$ $M^{-1}$) and substantial affinity for $Mg^{2+}$ ($K_{Mg} > 10^4$ $M^{-1}$). By contrast, $Ca^{2+}$-specific sites are well-suited for $Ca^{2+}$-dependent regulatory roles, with moderate affinity for $Ca^{2+}$ ($K_{Ca} \approx 10^6$ $M^{-1}$) and low affinity for $Mg^{2+}$ ($K_{Mg} < 10^3$ $M^{-1}$). The high-affinity EF-hand motif in Phl p 7 does not fit neatly into either category. Although it would certainly qualify as a $Ca^{2+}$-specific site with a $Ca^{2+}$ binding constant

of $1.7 \times 10^6$ $M^{-1}$, the corresponding $Mg^{2+}$ binding constant, at $2.8 \times 10^4$ $M^{-1}$, is more typical of a $Ca^{2+}/Mg^{2+}$ site. This unusually high $Mg^{2+}$ affinity is presumably a consequence of the pentacarboxylate ligand array. In rat $\beta$-parvalbumin, for example, the S55D mutation increases the $Mg^{2+}$ binding constant for the CD site from $9.4 \times 10^3$ to $4.5 \times 10^4$ $M^{-1}$.

The ratio of $Ca^{2+}$ and $Mg^{2+}$ binding constants for an EF-hand motif is commonly $1-2 \times 10^4$. Judged by this criterion, both sites in Phl p 7 are distinctly atypical. Site 2 exhibits a ratio of just 60. Two factors are responsible for this anomalously low value. First, whereas the intrinsic $Ca^{2+}$ affinity of site 2 is seriously depressed by the requirement for an energetically costly conformational change, the intrinsic $Mg^{2+}$ affinity is not. Second, the pentacarboxylate ligand array confers exceptionally high intrinsic $Mg^{2+}$ affinity on the site. In contrast to site 2, the ratio of $Ca^{2+}$ and $Mg^{2+}$ binding constants observed for site 1 is unusually large, at $4.7 \times 10^4$. The intrinsic $Ca^{2+}$ affinity of site 1 is heightened by the positively cooperative interaction with site 2. Presumably, it is this enhancement of $Ca^{2+}$ affinity that produces the elevated binding constant ratio.

The high affinity associated with the first $Mg^{2+}$ binding event has important biological ramifications. When 1 mM $Mg^{2+}$ is present, binding of $Ca^{2+}$ is strongly discouraged (Figure 4, dotted line). In the absence of other factors, the Phl p 7 binding sites would be largely unoccupied by $Ca^{2+}$ at physiological concentrations of the ion. However, the positively cooperative $Ca^{2+}$ binding signature and concomitant exposure of apolar surface are strongly suggestive of a regulatory function, as proposed previously by other investigators (*11, 18*). In the presence of an appropriate biological target protein or peptide, the $Ca^{2+}$ binding curve would be shifted back into the physiologically relevant range. The dashed line in Figure 4 is the predicted $Ca^{2+}$ binding curve for Phl p 7 in the presence of 1 mM $Mg^{2+}$ and a 10 $\mu$M target having an association constant for $Ca^{2+}$-bound Phl p 7 of $10^7$ $M^{-1}$.

## CONCLUSIONS

Although it crystallizes as a domain-swapped dimer at low pH, Phl p 7 is monomeric in solution at neutral pH in both the apo and $Ca^{2+}$-bound forms. The apoprotein exhibits noteworthy thermal stability, denaturing at 78.4 °C in phosphate-buffered saline at pH 7.4. This stability reflects the small denaturational heat capacity increment, 0.20 kcal $mol^{-1}$ $K^{-1}$, in turn a reflection of a small hydrophobic core. $Ca^{2+}$ binding is cooperative and linked to the exposure of apolar surface area, consistent with a $Ca^{2+}$-dependent regulatory function. By contrast, $Mg^{2+}$ binding is noncooperative and evidently unaccompanied by significant conformational change. EF-hand 2 in Phl p 7 is noteworthy for the presence of anionic side chains at five of the coordination sites in the binding loop. On the basis of the performance of this ligand constellation in the parvalbumin background, we propose that site 2 is preferentially occupied by divalent ions. Although the intrinisically high $Ca^{2+}$ affinity of this site is veiled by the energetic penalty attendant to exposure of hydrophobic surface, the site exhibits an inordinately high affinity for $Mg^{2+}$. In fact, in the absence of a suitable biological target, the $Mg^{2+}$ affinity is sufficiently high that it would discourage $Ca^{2+}$ binding at physiological concentrations of the two ions.

## REFERENCES


1. Kuby, J. (1992) *Immunology*, Freeman, New York.
2. Kay, A. B. (2001) Allergy and allergic diseases. First of two parts. *N. Engl. J. Med. 344*, 30–37.
3. Kay, A. B. (2001) Allergy and allergic diseases. Second of two parts. *N. Engl. J. Med. 344*, 109–113.
4. Valenta, R., Hayek, B., Seiberler, S., Bugajska-Schretter, A., Niederberger, V., Twardosz, A., Natter, S., Vangelista, L., Pastore, A., Spitzauer, S., and Kraft, D. (1998) Calcium-binding allergens: From plants to man. *Int. Arch. Allergy Immunol. 117*, 160–166.
5. Tinghino, R., Twardosz, A., Barletta, B., Puggioni, E. M., Iacovacci, P., Butteroni, C., Afferni, C., Mari, A., Hayek, B., Di, F. G., Focke, M., Westritschnig, K., Valenta, R., and Pini, C. (2002) Molecular, structural, and immunologic relationships between different families of recombinant calcium-binding pollen allergens. *J. Allergy Clin. Immunol. 109*, 314–320.
6. Celio, M. R., Pauls, T., and Schwaller, B. (1996) *Guidebook to the Calcium-Binding Proteins*, Oxford University Press, New York.
7. Kretsinger, R. H., and Nockolds, C. E. (1973) Carp muscle calcium-binding protein. II. Structure determination and general description. *J. Biol. Chem. 248*, 3313–3326.
8. Kretsinger, R. H. (1980) Structure and evolution of calcium-modulated proteins. *CRC Crit. Rev. Biochem. 8*, 119–174.
9. Kawasaki, H., and Kretsinger, R. H. (1995) Calcium-binding proteins 1: EF-hands. *Protein Profile 2*, 297–490.
10. McPhalen, C. A., Strynadka, N. C. J., and James, M. N. G. (1991) Calcium-binding sites in proteins: A structural perspective. *Adv. Protein Chem. 42*, 77–144.
11. Engel, E., Richter, K., Obermeyer, G., Briza, P., Kungl, A. J., Simon, B., Auer, M., Ebner, C., Rheinberger, H. J., Breitenbach, M., and Ferreira, F. (1997) Immunological and biological properties of Bet v 4, a novel birch pollen allergen with two EF-hand calcium-binding domains. *J. Biol. Chem. 272*, 28630–28637.
12. Ledesma, A., Villalba, M., Batanero, E., and Rodriguez, R. (1998) Molecular cloning and expression of active Ole e 3, a major allergen from olive-tree pollen and member of a novel family of $Ca^{2+}$-binding proteins (polcalcins) involved in allergy. *Eur. J. Biochem. 258*, 454–459.
13. Rozwadowski, K., Zhao, R., Jackman, L., Huebert, T., Burkhart, W. E., Hemmingsen, S. M., Greenwood, J., and Rothstein, S. J. (1999) Characterization and immunolocalization of a cytosolic calcium-binding protein from *Brassica napus* and *Arabidopsis* pollen. *Plant Physiol. 120*, 787–798.
14. Suphioglu, C., Ferreira, F., and Knox, R. B. (1997) Molecular cloning and immunological characterisation of Cyn d 7, a novel calcium-binding allergen from Bermuda grass pollen. *FEBS Lett. 402*, 167–172.
15. Okada, T., Zhang, Z., Russell, S. D., and Toriyama, K. (1999) Localization of the $Ca^{2+}$-binding protein, Bra r 1, in anthers and pollen tubes. *Plant Cell Physiol. 40*, 1243–1252.
16. Twardosz, A., Hayek, B., Seiberler, S., Vangelista, L., Elfman, L., Gronlund, H., Kraft, D., and Valenta, R. (1997) Molecular characterization, expression in *Escherichia coli*, and epitope analysis of a two EF-hand calcium-binding birch pollen allergen, Bet v 4. *Biochem. Biophys. Res. Commun. 239*, 197–204.
17. Hayek, B., Vangelista, L., Pastore, A., Sperr, W. R., Valent, P., Vrtala, S., Niederberger, V., Twardosz, A., Kraft, D., and Valenta, R. (1998) Molecular and immunologic characterization of a highly cross-reactive two EF-hand calcium-binding alder pollen allergen, Aln g 4: Structural basis for calcium-modulated IgE recognition. *J. Immunol. 161*, 7031–7039.
18. Neudecker, P., Nerkamp, J., Eisenmann, A., Nourse, A., Lauber, T., Schweimer, K., Lehmann, K., Schwarzinger, S., Ferreira, F., and Rosch, P. (2004) Solution structure, dynamics, and hydrodynamics of the calcium-bound cross-reactive birch pollen allergen Bet v 4 reveal a canonical monomeric two EF-hand assembly with a regulatory function. *J. Mol. Biol. 336*, 1141–1157.
19. Verdino, P., Westritschnig, K., Valenta, R., and Keller, W. (2002) The cross-reactive calcium-binding pollen allergen, Phl p 7, reveals a novel dimer assembly. *EMBO J. 21*, 5007–5016.
20. Verdino, P., Barderas, R., Villalba, M., Westritschnig, K., Valenta, R., and Keller, W. (2008) Three-dimensional structure of the cross-reactive pollen allergen Che a 3: Visualizing cross-reactivity on the molecular surfaces of weed, grass, and tree pollen allergens. *J. Immunol. 180*, 2313–2321.
21. Marsden, B. J., Hodges, R. S., and Sykes, B. D. (1988) $^1$H NMR studies of synthetic peptide analogues of calcium-binding site III of rabbit skeletal troponin C: Effect on the lanthanum affinity of

the interchange of aspartic acid and asparagine residues at the metal ion coordinating positions. *Biochemistry 27*, 4198–4206.
22. Henzl, M. T., Hapak, R. C., and Goodpasture, E. A. (1996) Introduction of a fifth carboxylate ligand heightens the affinity of the oncomodulin CD and EF sites for $Ca^{2+}$. *Biochemistry 35*, 5856–5869.
23. Henzl, M. T., Agah, S., and Larson, J. D. (2004) Rat α- and β-parvalbumins: Comparison of their pentacarboxylate and site-interconversion variants. *Biochemistry 43*, 9307–9319.
24. Lee, Y. H., Tanner, J. J., Larson, J. D., and Henzl, M. T. (2004) Crystal structure of a high-affinity variant of rat α-parvalbumin. *Biochemistry 43*, 10008–10017.
25. Weber, G., and Young, L. (1964) Fragmentation of bovine serum albumin by pepsin. I. The origin of the acid expansion of the albumin molecule. *J. Biol. Chem. 239*, 1415–1423.
26. Schuck, P., Perugini, M. A., Gonzales, N. R., Howlett, G. J., and Schubert, D. (2002) Size-distribution analysis of proteins by analytical ultracentrifugation: Strategies and application to model systems. *Biophys. J. 82*, 1096–1111.
27. Haner, M., Henzl, M. T., Raissouni, B., and Birnbaum, E. R. (1984) Synthesis of a new chelating gel: Removal of $Ca^{2+}$ ions from parvalbumin. *Anal. Biochem. 138*, 229–234.
28. Henzl, M. T., Agah, S., and Larson, J. D. (2003) Characterization of the metal ion-binding domains from rat α- and β-parvalbumins. *Biochemistry 42*, 3594–3607.
29. Henzl, M. T., Larson, J. D., and Agah, S. (2003) Estimation of parvalbumin $Ca^{2+}$- and $Mg^{2+}$-binding constants by global least-squares analysis of isothermal titration calorimetry data. *Anal. Biochem. 319*, 216–233.
30. Henzl, M. T., Larson, J. D., and Agah, S. (2004) Influence of monovalent cation identity on parvalbumin divalent ion-binding properties. *Biochemistry 43*, 2747–2763.
31. Henzl, M. T., and Ndubuka, K. (2007) Low-affinity signature of the rat β-parvalbumin CD site. Evidence for remote determinants. *Biochemistry 46*, 23–35.
32. Daniel, E., and Weber, G. (1966) Cooperative effects in binding by bovine serum albumin. I. The binding of 1-aniline-8-naphthalenesulfonate. Fluorometric titrations. *Biochemistry 5*, 1893–1900.
33. Liu, Y., and Eisenberg, D. (2002) 3D domain swapping: As domains continue to swap. *Protein Sci. 11*, 1285–1299.
34. Niederberger, V., Hayek, B., Vrtala, S., Laffer, S., Twardosz, A., Vangelista, L., Sperr, W. R., Valent, P., Rumpold, H., Kraft, D., Ehrenberger, K., Valenta, R., and Spitzauer, S. (1999) Calcium-dependent immunoglobulin E recognition of the apo- and calcium-bound form of a cross-reactive two EF-hand timothy grass pollen allergen, Phl p 7. *FASEB J. 13*, 843–856.
35. Wyman, J., and Gill, S. C. (1990) *Binding and Linkage: Functional Chemistry of Biological Macromolecules*, University Science Books, Mill Valley, CA.
36. Reid, R. E., and Hodges, R. S. (1980) Cooperativity and calcium/magnesium binding to troponin C and muscle calcium binding parvalbumin: An hypothesis. *J. Theor. Biol. 84*, 401–444.
37. Reid, R. E. (1990) Synthetic fragments of calmodulin calcium-binding site III. A test for the acid pair hypothesis. *J. Biol. Chem. 265*, 5971–5976.
38. Procyshyn, R. M., and Reid, R. E. (1994) A structure/activity study of calcium affinity and selectivity using a synthetic peptide model of the helix-loop-helix calcium-binding motif. *J. Biol. Chem. 269*, 1641–1647.
39. Procyshyn, R. M., and Reid, R. E. (1994) An examination of glutamic acid in the -X chelating position of the helix-loop-helix calcium binding motif. *Arch. Biochem. Biophys. 311*, 425–429.
40. Ahmed, F. R., Rose, D. R., Evans, S. V., Pippy, M. E., and To, R. (1993) Refinement of recombinant oncomodulin at 1.30 Å resolution. *J. Mol. Biol. 230*, 1216–1224.
41. Declercq, J. P., Tinant, B., Parello, J., and Rambaud, J. (1991) Ionic interactions with parvalbumins. Crystal structure determination of pike 4.10 parvalbumin in four different ionic environments. *J. Mol. Biol. 220*, 1017–1039.

BI800620G